Bull. Mater. Sci., Vol. 34, No. 2, April 2011, pp. 183–189. © Indian Academy of Sciences.

Study of structural transformations and phases formation upon calcination of Zn–Ni–Al hydrotalcite nanosheets

ZHANSHUANG LI[†], YANCHAO SONG[†], JUN WANG[†,††,*], QI LIU[†], PIAOPING YANG[†] and MILIN ZHANG[†,††]

[†]College of Material Science and Chemical Engineering, Harbin Engineering University, Harbin 150001, P.R. China

[‡]The Key Laboratory of Superlight Materials and Surface Technology, Ministry of Education, 150001, P.R. China

MS received 21 March 2008; revised 23 December 2010

Abstract. **In this paper, we describe a general process for the synthesis of highly crystalline Zn–Ni–Al hydrotalcite-like materials. The structure and thermal decomposition of the prepared samples are studied by XRD, FT–IR, TG–DSC, SEM, TEM and N_2 adsorption/desorption. The morphology of large-sized, porous and hexagonal platelike Zn–Ni–Al hydrotalcite is affected by calcination temperature. BET specific surface area and pore volume are observed to increase with increase of the calcination temperature up to 700°C followed by a further decrease with increasing temperature.**

Keywords. **Nano materials; thermal analysis; X-ray analysis.**

1. Introduction

Layered double hydroxides (LDHs), also known as hydrotalcite-like compounds (HTLcs) have recently attracted increasing attention because of their potential applications in many areas. In particular, the industrial applications are ranging from ion exchange and waste water halogen scavenging to antacids in medicine. It is now well established that HTLcs are precursors for a wide range of mixed oxide catalysts (Cavani *et al* 1991). LDHs materials have the general formula, $\left[M^{2+}_{1-x}M^{3+}_{x}\,(OH)_2\right]^{x+}\left[X^{m-}_{x/m}\cdot nH_2O\right]$, where M^{2+} is a divalent (Mg, Mn, Fe, Co, Ni, Cu, Zn, Ga) and M^{3+} a trivalent metal cation (Al, Cr, Mn, Fe, Co, Ni, La). X^{m-} represents m-valence inorganic $\left(CO_3^{2-},\ OH^-,\ NO_3^-,\ SO_4^{2-},\ ClO_4^-\right)$, heteropolyacid $\left(PMo_{12}O_{40}^{3-}, PW_{12}O_{40}^{3-}\right)$, or even organic acid anions, x varies typically within 0·20 and 0·33 (Beaudot *et al* 2004). LDHs with brucite, coplanar octahedra $[M(OH)_6]$ like structure is a combination of host net obtained by the stacking of inorganic layers and chemical species trapped in the interlamellar domain. The simultaneous presence of divalent and trivalent metallic cations in these layers leads to a positive charge which is balanced by anionic species located in the interlamellar space with water molecules and carbonates (Iyi *et al* 2004). These materials can be prepared by different methods, such as coprecipitation (Choudary *et al* 2005), anion exchange (Reinholdt and Kirkpatrick 2006), reconstruction method (Carriazo *et al* 2006), hydrothermal method (Benito *et al* 2006a) and urea methods (Kloprogge *et al* 2006). In the same way, it is possible to synthesize LDHs containing three or more cations in the layers. Decomposition of LDHs at moderate temperatures leads to mixed oxides with high specific surface area and reactivity that are of interest in catalytic applications.

Zn–Ni–Al hydrotalcite is attractive as a catalyst or catalyst support because of its low cost, highly active alkali centre and stable oxides obtained after thermal treatments. However, the activity of these catalysts or catalyst supports is limited by their acid-base or redox properties, which depend on their surface area and crystallinity. The preparation of Zn–Ni–Al hydrotalcite has been reported (Benito *et al* 2006b), however, the pore size distribution of the sample is not uniform. Hydrothermal method can provide mild reactive condition which is favourable in controlling the morphology and properties of hydrotalcite (Wang *et al* 2006, 2008; Xu *et al* 2006; Gunawan and Xu 2009). This paper describes the structure and thermal decomposition of Zn–Ni–Al hydrotalcite nanosheets. It was observed that during calcinations, as the heating temperature increased, the characteristic peaks of LDHs gradually disappeared. Broadening of the crystalline reflections of the diffraction peaks in the thermally treated material indicates a loss of some degree of crystallinity (Malak-Polaczyk *et al* 2010). The decomposition reaction can be classified into (i) the loss of interlayer water and an intermediate structure is formed, and (ii) the collapse of the layered structure and the decomposition of the anions. In the present work, the condensation of hydroxyls in the octahedral layers will lead to creation of a more open meso/macrostructure. A three-dimensional structure between rock salt and spinel is formed (Rey *et al* 1992), which is the

*Author for correspondence (junwang@hrbeu.edu.cn)

base product for catalyst fabrication. Further thermal treatment results in a decrease of the surface area, caused by the formation of oxide sintering and aggregation. In addition, adsorption/desorption is carried out to determine the porous properties of the samples.

2. Experimental

2.1 *Synthesis of Zn–Ni–Al hydrotalcite*

The Zn–Ni–Al hydrotalcite was synthesized through the hydrothermal reaction of solutions A and B. Solution A was prepared by mixing 0·02 M $Al(NO_3)_3$, 0·04 M $Ni(NO_3)_2$ with 0·02 M $Zn(CH_3COOH)_2$ in distilled water. Solution B consisted of 0·05 M Na_2CO_3 and 0·18 M NaOH. Solutions A and B were added dropwise into a three-necked flask at 85°C under strong stirring for 1 h, and the mixture solution (pH = 11) was transferred into a stainless steel autoclave and heated at 120°C for 6 h. The resulting slurry was filtered and washed thoroughly with distilled water until the pH was 7·0. A green colour product was obtained after drying at 100°C for 8 h. The final product was calcined in a muffle furnace for 6 h from 200–900°C.

2.2 *Characterization*

Powder X-ray diffraction (XRD) patterns were collected on a Rigaku D/max-IIIB diffractometer using Cu Kα radiation (λ = 1·5406 Å). Fourier transform infrared (FT–IR) spectrum was recorded on a Nicolet 5DX spectrophotometer using KBr pellet technique. Transmission electron microscopy (TEM) experiment was performed on a PHILIPS CM 200 FEG electron microscope with an acceleration voltage of 200 kV. Scanning electron microscopy (SEM) was performed on a Japan JEOL JSM-6480A instrument at an acceleration voltage of 20 kV and a working distance of 10 mm. Thermogravimetry–differential scanning calorimetry (TG–DSC) was performed on a NETZSCH STA 409PC thermoanalyser in the temperature range of 40∼600ºC with a heating rate of 10ºC/min. The metal contents in the hydrotalcite were determined by inductively coupled plasma-mass spectrometry on a XSeriesΠ ICP-MS instrument. The Brunauer–Emmett–Teller (BET) equation was used to calculate the specific surface area. Pore size distributions were obtained using the Barrett–Joyner–Halenda (BJH) method from the desorption branch of N_2 adsorption/desorption, the isotherm measured on Micromeritics ASAP2010.

3. Results and discussion

3.1 *Thermal analysis*

To examine the thermal stability of Zn–Ni–Al hydrotalcite during calcination, TG–DSC and DTA curves were presented in figure 1. According to the TG analysis, the thermal decomposition process could be described in two consecutive overlapped steps with a total weight loss of 22·57%. The first weight loss of 9·08% occurred between 40 and 240°C (endothermic peaks appear at 221°C as shown in DTA curve) corresponding to the removal of water molecules physically adsorbed on the external surface of the crystallites (Ram Reddy *et al* 2006). The structure change after removing water was confirmed by XRD patterns at 200°C (see figure 2). The second loss of 14·39% between 240 and 600°C was ascribed to the removal of interlayer water molecules, dehydroxylation and decarbonation of the layers. The endothermic peak at 359°C with a shoulder peak might suggest the overlapped process of dehydroxylation and decarbonation. Correlation of thermal analysis with XRD

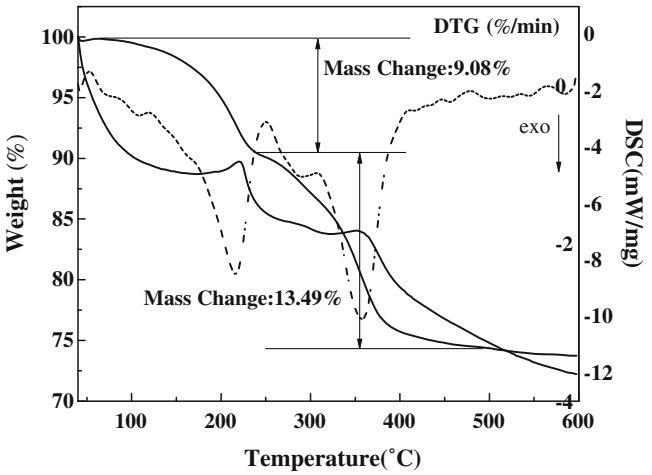

Figure 1. TG–DSC curves of Zn–Ni–Al hydrotalcite.

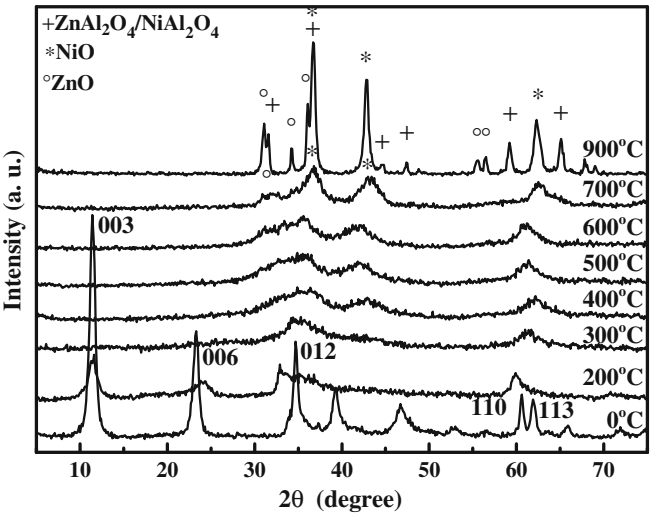

Figure 2. XRD patterns of Zn–Ni–Al hydrotalcite calcined at different temperatures.

patterns revealed the formation of oxide under dehydroxylation and decarbonation effect. Peaks in DSC curves were also consistent with the thermal behaviour of the sample.

3.2 *Powder X-ray diffraction*

The XRD patterns of as-synthesized and calcined samples in the 200–900°C range are presented in figure 2. As can be seen, highly crystallized Zn–Ni–Al hydrotalcite was synthesized. The disappearance of (003) reflections suggested the decrease of crystallinity. The (110) inflection could be observed for sample calcined at 200°C which demonstrated that the lamellar structure of hydrotalcite still existed below this temperature. When calcined at 300°C, parts of diffraction peaks disappeared, indicating that the structure of hydrotalcite began to decompose. Furthermore, the non-existence of peak (006) also confirmed the collapse of the layered structure.

Broad peak of NiO appeared when the sample calcined over 300°C and the intensity of the peaks increased with increasing temperature. Characteristic peaks at $2\theta = 35{\cdot}59°$, $42{\cdot}0°$ and $61{\cdot}16°$ were due to NiO crystal phase formation during calcination process. Diffraction peak ($2\theta = 31{\cdot}71°$) of ZnO crystal could be observed in the sample calcined at 600°C. The appearance of the oxide also indicated the partial disorder of the structure. A mixture of ZnO, NiO and $NiAl_2O_4$ ($ZnAl_2O_4$) ($2\theta = 56{\cdot}30°$, $36{\cdot}20°$) were formed when the temperature reached 900°C (Mavis and Akine 2006). The above results demonstrated the gradual transformation process of the structure and composition of hydrotalcite. At higher temperature (900°C), original layered hydrotalcite nanosheets were converted completely to the mixture of oxide and spinel. Besides, although thermal decomposition of the Zn–Ni–Al hydrotalcite produce some aluminum-containing phase, it was not observed from our XRD patterns; we surmised that it may exist as an amorphous phase or as a solid solution of aluminum in zincite. The proposed cation composition of the precursor is $Zn_{0{\cdot}031}Ni_{0{\cdot}064}Al_{0{\cdot}028}$, indicating that the Zn/Ni/Al ratio in the precursor was similar to that in the initial synthesis mixture.

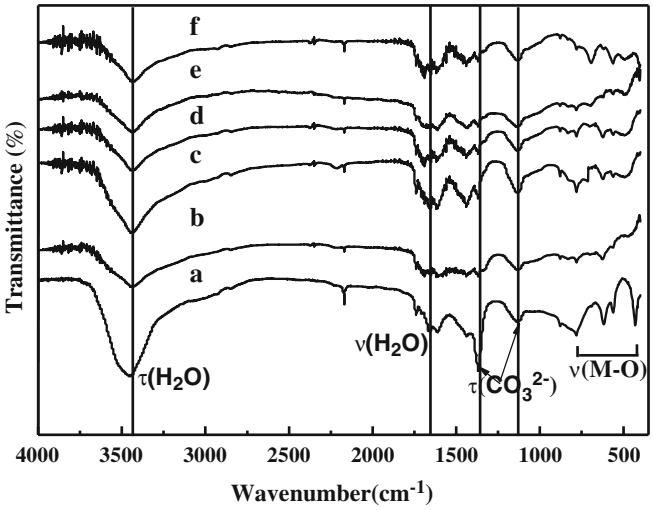

Figure 3. FT–IR spectra of as-synthesized sample, a and samples calcined at different temperatures (b: 200, c: 300, d: 400, e: 500, f: 600°C).

3.3 *Fourier transform–infrared (FT–IR) spectroscopy*

The FT–IR spectra of the as-synthesized Zn–Ni–Al hydrotalcite showed broad band at 3442 cm^{-1}, which is assigned to the stretching mode of hydroxyl groups of Zn–Ni–Al hydrotalcite and interlayer water (Das *et al* 2006). In addition, the weak band at 1645 cm^{-1} was due to H_2O bending vibration in the interlayer space (Chen *et al* 2006). The sharp, intense

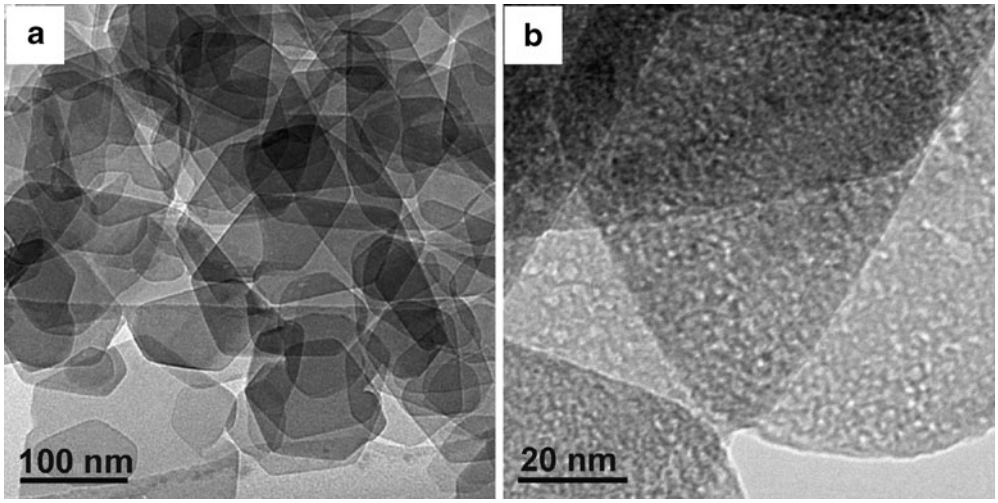

Figure 4. TEM images of Zn–Ni–Al hydrotalcite with different magnification times.

vibrational band of carbonates (antisymmetric stretching, ν_3) that appears at 1370 and 1122 cm^{-1} could be assigned to interlayer carbonates (chelating or bridging bidentate) (figure 3, spectrum a). Peaks at 775 cm^{-1}, 606 cm^{-1}, 550 cm^{-1}, 430 cm^{-1} were assigned to vibrational modes of M–O, M–O–M, and O–M–O species in the interlayers (Rivera *et al* 2006). Heating the sample at 300°C led to a slight modification of the spectrum (figure 3, spectrum c). The carbonate and –OH bands are sharpened and slightly reduced in intensity. These results are indicative of the onset of sample decomposition starting at this temperature. This is consistent with the TG–DSC results, which showed removal of water molecules from the interlayer, a partial dehydroxylation, and a decomposition of carbonate beginning at this temperature. The increase of calcination temperature led to dramatic changes in the sample background spectrum (figure 3, spectrum c, d, e, f). The OH and CO_3^{2-} vibration bands have drastically decreased in intensity, which was probably due to the removal of interlayer water and CO_2 (Jaubertie *et al* 2006).

3.4 *TEM images*

Figure 4 shows TEM images of as-synthesized Zn–Ni–Al hydrotalcite. It could be clearly seen that the morphology of these LDHs particles exhibited hexagonal platelet-like with a diameter of 200 nm (figure 4(a)) (Kuśtrowski *et al* 2004). The formation process was moved as follows: the small crystal nuclei grew slowly and formed to small uniform crystal, then led to the hexagonal nanosheet under mild hydrothermal treatment. The enlarged TEM image of the as-synthesized sample (figure 4(b)) indicated that the as-synthesized hydrotalcite nanosheets were formed by secondary nanoparticles, of size about 10 nm. This particle volume provided large surface area for the improvement of catalytic activity.

3.5 *SEM images*

The effect of calcination temperature on the morphology of sample was investigated by SEM and the results are shown

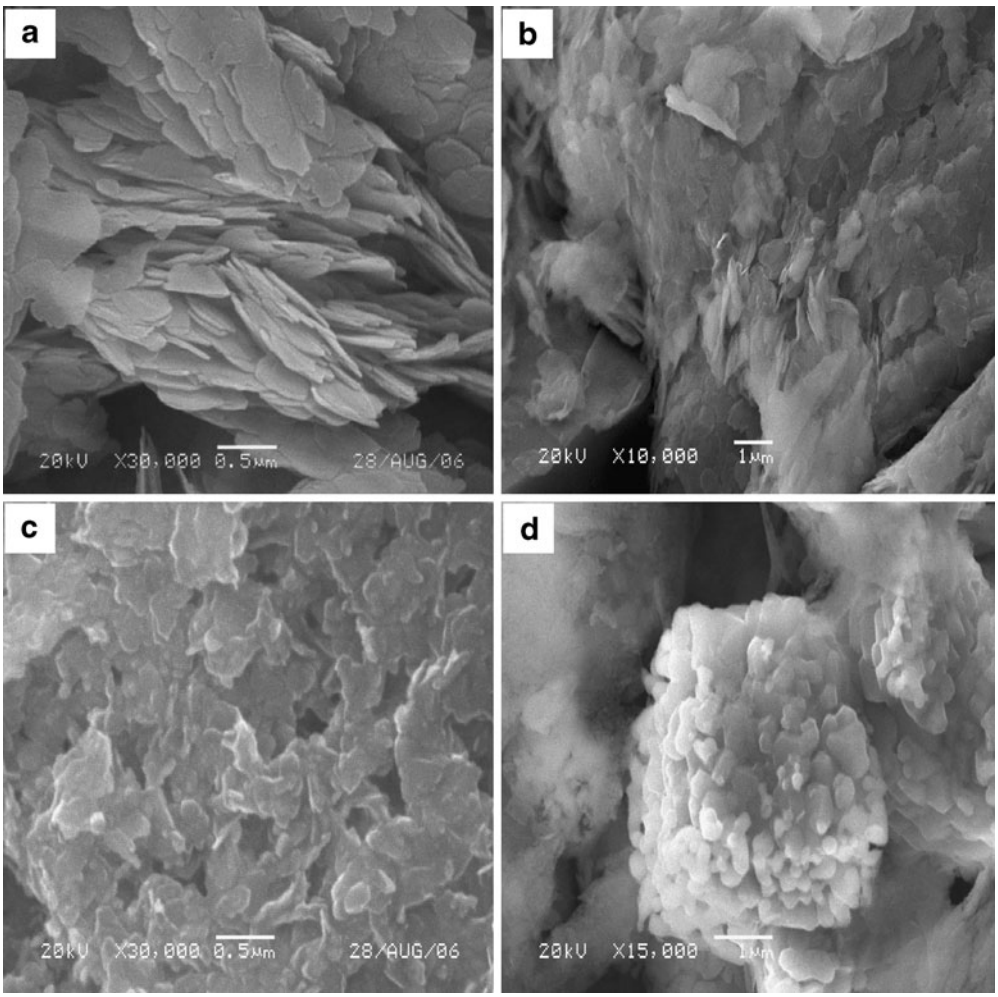

Figure 5. SEM images of Zn–Ni–Al hydrotalcite: (**a**) as-synthesized sample; (**b**) calcined sample at 200°C; (**c**) calcined sample at 400°C and (**d**) calcined sample at 700°C.

in figure 5. It is observed that the as-synthesized sample has uniform hexagonal nanosheets with an average diameter of about 170 nm (figure 5(a)). When the temperature was increased, some water began to evaporate, the construction of as-synthesized sample became more compact than usual. In figure 5b, the nanosheets became irregular; it was difficult to observe the LDHs of hexagonal, but there were still some monodisperse nanosheets. When calcined at 400°C (in figure 5(c)), the oxide agglomerated and formed to particles with irregular shape and pores. The interconnection of the irregular LDHs nanosheets led to high surface area and large volume. As shown in figure 5(d), the mixture of ZnO, NiO and $NiAl_2O_4$ ($ZnAl_2O_4$) were formed when calcined at 700°C, and Zn–Ni–Al hydrotalcite was converted to oxide completely. These particles stacked each other with an irregular size of about 200–500 nm. The increased size of these particles could be ascribed to the growth of crystal with increased temperature.

3.6 *N_2 adsorption and desorption*

In order to study the influence of calcination temperature on the textural properties of Zn–Ni–Al hydrotalcite, N_2 adsorption experiment was done (see figure 6). The shapes of all the isotherms were of type IV according to the IUPAC classification and represented a mesoporous adsorbent with strong adsorbent–adsorbate interaction (Kannan *et al* 2005). The isotherms showed that desorption started immediately after completion of adsorption. The hysteresis is associated with capillary condensation in the mesostructure, which may relate to the shape and homogeneity of the pore size. The pore size distribution was determined by BJH method and the results are shown in the inset of figure 6. A narrow size distribution of small and thin plate-like particles was obtained from as-synthesized sample, whereas a broader distribution of pores from sample calcined at 200°C (figure 6(b)). The pore diameter distribution becomes more complex at higher

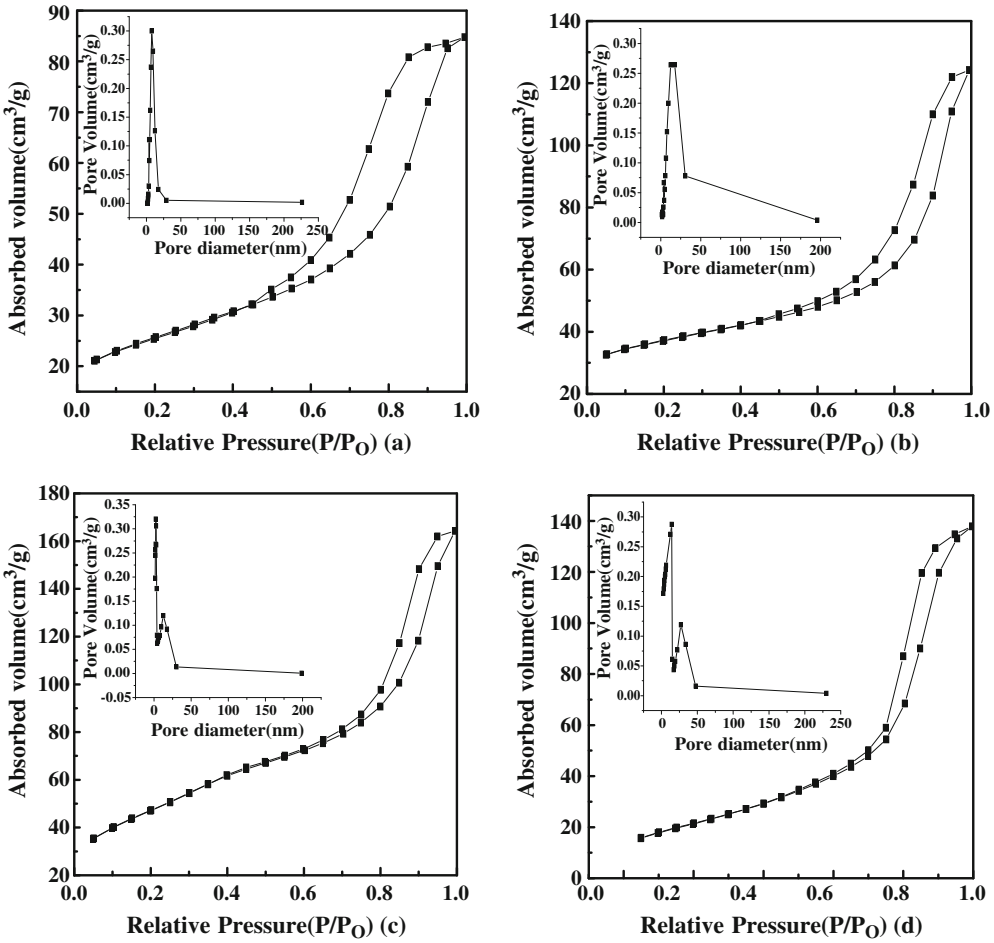

Figure 6. N_2 adsorption/desorption isotherms at 77 K of Zn–Ni–Al hydrotalcite calcined at different temperatures: ((**a**) 0°C; (**b**) 200°C; (**c**) 400°C; (**d**) 700°C). Inset: pore size distribution (BJH, desorption branch of isotherm).

Table 1. Specific surface areas and pore parameters of Zn–Ni–Al hydrotalcite calcined at different temperatures.

Calcination temperature °C	S_{BET} (BET surface area) (m^2/g)	V_P (Pore volume) (cm^3/g)	d_P (Pore diameter) (nm)
0	86·1	0·131	6·111
200	117	0·193	6·577
400	170	0·254	6·007
700	133	0·226	6·347

calcination temperature, two kinds of pore diameter distribution were observed from figures 6(c) and (d). These changes were attributed to the different morphologies of the pores at different calcination temperatures. At lower calcination temperature, platelet agglomeration resulted in the formation of spongy particles (Carja *et al* 2001), whereas sintering phenomenon became obvious at higher calcination temperature. The above results coincided with SEM images.

Table 1 lists S_{BET}, V_p and d_p for as-synthesized and calcined samples. The surface area of the hydrotalcite samples was observed to change from 86·1 to 117, 170 and 133 m^2/g with an increase in calcination temperature. The V_p value was changed from 0·131 to 0·254 cm^3/g on increasing the temperature from 0 to 450°C. It can be concluded that the removal of layered water and carbonate led to the increase of S_{BET} and V_p below 400°C. At higher calcination temperature (700°C), the values of S_{BET} and V_p decreased. The decrease of S_{BET} and V_p was ascribed to the formation of oxide accompanied by sintering and aggregation.

4. Conclusions

The XRD studies presented in this paper, complemented by additional techniques, indicated structural transformations and phases formed upon calcination of Zn–Ni–Al hydrotalcite nanosheets. TEM analysis demonstrated the formation of pure hydrotalcite with uniform size, which was porous and well-crystallized. The thermal properties of the as-synthesized sample were consistent with the inherent structure of hydrotalcite. With the increase of calcination temperature, the uniform hydrotalcite nanosheets disappeared gradually and surface-ragged while irregular particles of oxide appeared. For sample calcined at 700°C, the aggregation of the oxide particles was observed clearly. N_2 adsorption/desorption studies revealed that Zn–Ni–Al hydrotalcite nanosheets were porous material. The pore volume and S_{BET} of the calcined product increased greatly with an increase in calcination temperature and reached the highest value of pore volume (0·254 cm^3/g) and S_{BET} (170 m^2/g) at 400°C. The decomposition of hydrotalcite at moderate temperatures leads to mixed oxides of high specific surface area and reactivity that are of interest in catalytic applications.

Acknowledgements

We gratefully acknowledge the support of this research by the Key Technology R&D Program of Heilongjiang Province (TB06A05), the Fundamental Research Funds of the Central University, and the Science Fund for Young Scholar of Harbin City (2004AFQXJ038).

References

Beaudot P, De Roy M E and Besse J P 2004 *J. Solid State Chem.* **177** 2691

Benito P, Labajos F M and Rives V 2006a *Cryst. Growth Des.* **6** 1961

Benito P, Labajos F M and Rives V 2006b *J. Solid State Chem.* **179** 3784

Carja G, Nakamura R, Aida T and Niiyama H 2001 *Micropor. Mesopor. Mater.* **47** 275

Carriazo D, Domingo C, Martin C and Rives V 2006 *Inorg. Chem.* **45** 1243

Cavani F, Trifirò F and Vaccari A 1991 *Catal. Today* **11** 173

Chen C X, Xu C H, Feng L R, Qiu F L, Suo J S and Mole J 2006 *Catal A: Chem.* **252** 171

Choudary B M, Ranganath K V S, Jagajit Y and Lakshmi Kantam M 2005 *Tetrahedron Lett.* **46** 1369

Das J, Das D and Parida K M 2006 *J. Colloid Interface Sci.* **301** 569

Gunawan P and Xu R 2009 *Chem. Mater.* **21** 781

Iyi N, Matsumoto T, Kaneko Y and Kitamura K 2004 *Chem. Mater.* **16** 2926

Jaubertie C, Holgado M J, San Roman M S and Rives V 2006 *Chem. Mater.* **18** 3114

Kannan S, Dubey A and Knozinger H 2005 *J. Catal.* **231** 381

Kloprogge J T, Hickey L, Trujillano R, Holgado M J, San Roman M S, Rives V, Martens W N and Frost R L 2006 *Cryst. Growth Des.* **6** 1533

Kuśtrowski P, Chmielarz L, Bożek E, Sawalha M and Roessner F 2004 *Mater. Res. Bull.* **39** 263

Malak-Polaczyk A, Vix-Guterl C and Frackowiak E 2010 *Energy Fuels* **24** 3346

Mavis B and Akinc M 2006 *Chem. Mater.* **18** 5317

Ram Reddy M K, Xu Z P, Lu G Q and Diniz da Costa J C 2006 *Ind. Eng. Chem. Res.* **45** 7504

Rey F, Fornés V and Rojo J M 1992 *J. Chem. Soc., Faraday Trans.* **88** 2233

Reinholdt M X and Kirkpatrick R J 2006 *Chem. Mater.* **18** 2567

Rivera J A, Fetter G and Bosch P 2006 *Micropor. Mesopor. Mater.* **89** 306

Wang Y G, Cheng L and Xia Y Y 2006 *J. Power Sources* **153** 191

Wang J, You J, Li Z S, Yang P P, Jing X Y, Cao D X and Zhang M L 2008 *Solid State Sci.* **10** 1093

Xu Z P, Stevenson G S, Lu C Q, Lu G Q, Bartlett P F and Gray P P 2006 *J. Am. Chem. Soc.* **128** 36